UNIVERSITÀ DEGLI STUDI DI TORINO

Design of High Surface Area Poly(Ionic Liquid)s to Convert Carbon Dioxide into Ethylene Carbonate

Alessandro Dani,[a] Elena Groppo,[a] Claudia Barolo,[a] Jenny G. Vitillo,[a,b] and Silvia Bordiga*[a]

A series of porous poly(ionic liquid)s (PILs) were synthesized using an innovative method which involves the synthesis of a non-ionic co-polymer of divinylbenzene and vinylimidazole, followed by an alkylation step to introduce the Ionic Liquid functionality in the polymeric matrix. This synthetic strategy allowed to obtain tuneable imidazolium type PILs having simultaneously high surface area and exposed ionic moieties. A set of PILs was obtained changing systematically the alkyl chains, the anions and the cross-link degree. This approach allowed to elucidate the effect of each synthetic variable on the catalytic performances of PILs towards carbon dioxide cycloaddition reaction in very mild conditions (room temperature and low pressure). Finally, in-situ FTIR spectroscopy allowed to establish a relation between structure of PILs and their catalytic properties.

1 Introduction

Carbon dioxide is one of the most abundant human activity waste and, being a renewable non-toxic sources of C1, its use as a chemical feedstock is gaining interest, since it would reintegrate it in the industrial processes.[1-3] The level of carbon dioxide in the atmosphere is reaching a concentration of almost 400 ppm,[4] corresponding to an excess of about 1000 Gtons with respect to the pre-industrial age.[5] This number will increase in the years to come, due to the industrial development and increasing economy, in particular in the developing nations. The control and the depression of the carbon dioxide emission is one of the big challenge of these decades, at least until all the carbon based energy sources will be replaced with renewable energies.[6-8]

In general terms, the low energy content of carbon dioxide implies that its conversion in anything else is considered an energy demanding process.[9] A possible route to promote CO_2 conversion is to exploit the electrophilic character of the carbon atom (carbon dioxide can be considered the dehydrated form of carboxylic acid) reacting it with nucleophilic molecules through a coupling reaction. Epoxides or Grignard reagents respond to both requirements, being nucleophilic molecules and with a high potential energy.[9]

In our work we have considered the reaction between carbon dioxide and ethylene oxide, in order to obtain ethylene carbonate. This product have important application as organic solvent, electrolyte in Li-ion battery, and for cosmetic and pharmaceutical preparation.[7] Furthermore it is an important industrial intermediate for the synthesis of polycarbonate and polyurethane in green conditions[10] (i.e. avoiding the usage of phosgene and having only water as by-product). A large number of catalysts for the cycloaddition of CO_2 to epoxides have been proposed, ranging from heterogeneous catalysts (such as alkali metal salts[11, 12], organo-phosphorus compounds[13], metal oxides[14, 15], covalent organic framework (COF) functionalized with triazine[16]) to homogeneous catalysts (such as chromium complex in dichloromethane, isolated zinc complexes[17, 18] and ionic liquids in $scCO_2$[19-21]. Despite their high efficiency, homogeneous catalysts present the known disadvantages of difficult product separation and catalyst recycling. To overcome these drawbacks, many heterogeneous catalysts have been developed with the aim to retain the activity of their homogeneous counterpart, but improving the recyclability of the catalyst.[22] Among the systems proposed as catalysts for carboxylation of epoxides, ionic liquids (ILs) are recognized as the most efficient ones.[3] ILs possess interesting properties since they show high chemical and thermal stability, selective solubility towards organic and inorganic materials and high reusability. Moreover, the high solubility of CO_2 in ILs affords the activation of the carbon dioxide towards the cycloaddition reaction.

The drawback of using ILs for the coupling between CO_2 and epoxides is mainly due to their high viscosity, that leads to low diffusion coefficient for the reagents, and therefore slow kinetic of the reaction.[23] This disadvantage can be partially overcome by the use of poly(ionic liquid)s (PILs). These polymers have IL moieties as building units, which do not require solvents and, with opportune modifications of the polymeric structure, can lead to high porous materials. The achieved heterogeneous structure allow an easy diffusion of the reagents inside the catalyst, leading to an improvement of the reaction kinetics.[24] The first study on PILs as catalysts for coupling of carbon dioxide and ethylene carbonate was done by Xie and co-workers.[24] Later, further catalytic studies were reported on systems obtained by supporting on cross-linked polystyrene ionic liquids with different functionalities on the alkyl chain, such as hydroxyl groups[22, 25, 26], amino group[26] and carboxylic group[22, 27]. In those systems the performance in the CO_2 coupling reaction were found to decrease in the order: carboxylic group > hydroxyl group > amino group. All these studies were carried out using halogens as counter ions. Only recently PILs bearing BF_4^- and PF_6^- as counter ions were tested as catalysts in a coupling reaction.[28]

On the basis of the recent literature, we developed a systematic approach to understand the relation between PILs structure and their properties. The PILs were obtained following an original procedure that did not involve the polymerization of ionic monomers, but which uses a non-ionic vinylimidazole and divinylbenzene co-polymer as starting backbone. The co-polymers were subsequently modified using an alkylating agent capable to insert the ionic functionality in order to obtain the desired PILs. By using this approach it was possible to obtain a set of PILs with different anions and alkyl chains, but which retained the same starting polymeric matrix allowing an easy comparison. These PILs were tested in the coupling reaction between CO_2 and ethylene oxide in very mild conditions. The catalytic performances were tested by means of *in-situ* FTIR spectroscopy. This approach demonstrated to be very powerful to investigate systematically the effect of the counter anion (I^-, Br^- and BF_4^-), the length of the alkyl chain

(methyl and butyl) and the cross-link degree, on the catalytic performances of PILs.

A similar method to synthesize mesoporous PILs starting from non-ionic polymers was developed by Liu et al.[29] adopting solvothermal conditions. In respect to this approach, our synthetic strategy allows to perform the synthesis in milder conditions, avoiding the use of autoclaves, an aspect which is particularly important for up-scaled production. An alternative strategy to synthetize mesoporous PILs was followed by Weber et al. who synthetized mesoporous PILs starting from an IL monomer having also a cross-linker functionalityin presence of a hard-templating agent (silica) to create the mesoporosities.[30] By comparison, our synthetic route skips the challenging step required to selectively remove the templating agent. Concerning the post-polymerization step for the quaternarization, a similar approach was adopted in a previous study to get poly($eVIm^+Br^-$) from un-crosslinked poly(Vim). In that work, the quaternarization step was performed in solution because the starting poly(VIm) is soluble methanol.[31] On the contrary, in our study the quaternarization steps were performed in heterogeneous phase due to the cross-linked state of the starting polymers

2 Experimental

Materials

All solid and liquid starting materials were purchased from Sigma-Aldrich and used as received, unless differently specified. CO_2 was purchased from Praxair and ethylene oxide from Union Carbide. 1-vinylimidazole was used after distillation in vacuum (b.p. 85°C) and stored in fridge under inert atmosphere. Divinylbenzene was used after liquid-liquid extraction (three cycle of 5% NaOH in water solution followed by washing with water until neutral pH). DVB was stored in the fridge with anhydrous sodium sulfate to remove the residual moisture. Azobisisobutyronitrile was recrystallized from methanol and stored in the fridge.

Methods

All microwave reactions were performed in single-mode Biotage Initiator 2.5, by inserting all reagents in a sealed tube.

TGA measurements were performed under N_2 flow in the 30-500°C range (ramp 2°C/min) using an alumina pan, by means of a TA Q600 analyzer.

N_2 adsorption measurements at 77 K were performed using Autosorb iQ MP (Quantachrome). The samples were outgassed for 24 h at 50°C before the measurements. Surface area of the polymers was calculated by means of the BET and the Langmuir approximation in the standard p/p_0 range. Total pore volume was estimated as the volume occupied by liquid nitrogen at p/p_0 ~0.97.[32] Pore size distribution was estimated using QSDFT algorithm within the supplied software. Micropore volume is calculated using Harkins and Jura equation.[32, 33]

Morphological properties of the polymers were studied using SEM Zeiss EVO-50 XV, using a LaB_6 source operating at 30 kV current in high vacuum. EDX microanalysis was performed with OXFORD instrument.

In situ FT-IR spectra were recorded on a Bruker Vertex 70 spectrophotometer equipped with a MCT detector. Each spectrum was recorded at 2 cm^{-1} resolution and 32 scan in the range 4000-600 cm^{-1}. For all samples, a thin film of the polymeric powder was deposited on an IR transparent silicon plate and put in a cell equipped with two KBr windows, which allows the manipulation of the sample in controlled atmosphere while monitoring the FT-IR spectra. The sample cell is linked to a treatment line that permits to outgas the sample or dosing gas on it, while monitoring the evolution of the IR spectrum of the sample. The samples were outgassed at room temperature for 1 hour. Successively, 50 mbar of ethylene oxide were dosed followed by CO_2 dosage, to reach a final equilibrium pressure of 200 mbar. FT-IR spectra were collected at each step of the experiment and for the successive 14 hours to monitor the evolution of ethylene carbonate.

General synthesis of non-ionic polymer

The synthesis of the poly(DVB-co-VIm) was performed in a 100 mL three-neck round-bottom flask, using precipitation polymerization method. 64 mL of acetonitrile were used as solvent and 16 mL of toluene as porogenic agent. 40.0 mg of AIBN were used as initiator. The co-monomers, DVB and VIm, were poured in the reaction mixture using an amount that depends on the polymers, as described hereinafter. The reaction was conducted in nitrogen atmosphere at 80°C for 24 hours. The precipitated poly(DVB-co-VIm) was then filtered and washed three times with acetonitrile and acetone, in order to remove the unreacted monomers. The poly(DVB-co-VIm) was finally outgassed for 4 hours at room temperature.

Synthesis of 1: 1 mL of DVB and 1 mL of VIm were poured into the reaction flask. The product was obtained as a white fine powder with a yield of 27%. The thermal decomposition shows one step which starts at 350 °C and the material lose the 80% of its weight. Elemental analysis N: 2.47%, C: 87.0%, H: 7.65%. FT-IR frequencies: related to DVB 709 cm^{-1}, 795 cm^{-1}, 1509 cm^{-1}, 1487 cm^{-1}; related to VIm: 1225 cm^{-1}, 1110 cm^{-1}, 1081 cm^{-1}, 662 cm^{-1}.

Synthesis of 2: 0.6 mL of DVB and 1.4 mL of VIm were poured into the reaction flask. The product was obtained as a white powder with a yield of 23%. The thermal decomposition shows one step which starts at 350°C and the material lose the 80% of its weight. Elemental analysis N: 4.47%, C: 83.4%, H: 7.42%. FT-IR frequencies: related to DVB 709 cm^{-1}, 795 cm^{-1}, 1509 cm^{-1}, 1487 cm^{-1}; related to VIm: 1225 cm^{-1}, 1110 cm^{-1}, 1081 cm^{-1}, 662 cm^{-1}.

Synthesis of poly(DVB): 2mL of DVB were poured in the reaction flask. The product was obtained as a white powder with a yield of 65%. The thermal decomposition shows one step which starts at 350°C and the material lose the 80% of its weight. Elemental analysis N: 0.54%, C: 90.1%, H: 7.81%. FT-IR frequencies: related to DVB 709 cm^{-1}, 795 cm^{-1}, 1509 cm^{-1}, 1487 cm^{-1}

Synthesis of poly(VIm): 2mL of VIm were poured in the reaction flask. The product was obtained as a pale yellow powder with a yield of 91%. The thermal decomposition shows one step which starts at 200°C and the material lose the 85% of its weight. Elemental analysis N: 23.6 %, C: 54.8 %, H: 6.91 %. FTIR frequencies related to VIm: 1225 cm^{-1}, 1110 cm^{-1}, 1081 cm^{-1}, 662 cm^{-1}.

Synthesis of PILs

Synthesis of 1a and 2a

200 mg of the non-ionic polymer **1** or **2** were poured in a 5 mL hermetically sealed vial with 2 mL of methyl iodide and filled with nitrogen. The reaction was conducted in microwave at 100°C for 15 minutes. The poly(ionic liquid)s so obtained were filtered and washed three times with methanol and acetone, subsequently outgassed for 4 hours at room temperature.

1a The product was obtained as a yellow powder. The thermal decomposition shows two steps, the first starts at 150°C with a weight loss of 9.04%, the second step starts at 350°C and leads to the 20% of the starting weight. FT-IR band appear at 1157 cm^{-1}, while the FT-IR band at 1225 cm^{-1} present in the parent material **1** disappears.
2a The product was obtained as a yellow powder. The thermal decomposition shows two steps, the first starts at 150°C with a weight loss of 17.8%, the second step starts at 350°C and leads to the 20% of the starting weight. FT-IR band appears at 1157 cm^{-1}, while the FT-IR at 1225 cm^{-1} present in the parent material **2** disappears.

Synthesis of 1b and 2b
The synthesis follow the same steps as described above for **1a** and **2a**, except for the usage of 2 mL of butyl iodide as alkylating agent.

1b The product was obtained as a white powder. The thermal decomposition shows two steps, the first starts at 150°C with a weight loss of 14.3%, the second step starts at 350°C and leads to the 20% of the starting weight. FT-IR band appears at 1153 cm^{-1}, while the FT-IR band at 1225 cm^{-1} present in the parent material **1** disappears. EDX analysis shows 11.1% of iodine.
2b The product was obtained as a white powder. The thermal decomposition shows two steps, the first starts at 200°C with a weight loss of 21.4%, the second step starts at 350°C and leads to the 20% of the starting weight. FT-IR band appears at 1153 cm^{-1}, while the FT-IR at 1225 cm^{-1} present in the parent material **2** disappears. EDX analysis shows 20.1% of iodine.

Synthesis of 1c and 2c
The synthesis follow the same steps as described above, for **1a** and **2a**, except for the usage of 2 mL of butyl bromide as alkylating agent and a reaction temperature of 160°C.

1c The product was obtained as a yellow powder. The thermal decomposition shows two steps, the first starts at 150°C with a weight loss of 9.56%, the second step starts at 350°C and leads to the 20% of the starting weight. FT-IR band appears at 1154 cm^{-1}, while the FT-IR band at 1225 cm^{-1} present in the parent material **1** disappears.
2c The product was obtained as a yellow powder. The thermal decomposition shows two steps, the first starts at 150°C with a weight loss of 18.0%, the second step starts at 350°C and leads to the 20% of the starting weight. FT-IR band appears at 1155 cm^{-1}, while the FT-IR at 1225 cm^{-1} present in the parent material **2** disappears.

Synthesis of 1d and 2d
For the anion exchange, 200 mg of **1a** or **2a** were poured in a Buchner funnel with a sintered glass disk (P5). 20 mL of a saturated solution of $NaBF_4$ in methanol were flushed on PIL during 24 hours. When the sample turned from pale yellow to bright white the exchange step is considered finished. The **1d** and **2d** so obtained were filtered and washed three times with methanol and acetone, subsequently outgassed for 4 hours at room temperature.

1d The product was obtained as a white powder. The thermal decomposition of the PIL shows two subsequent steps. The first starts at 323°C, with a weight loss of 11.2%. The second step starts at 402°C and lead to the 17.3% of the starting weight. FT-IR bands assigned to BF_4^- anion appear at 1060 cm^{-1} and 3152 cm^{-1}. The achievement of the ion exchange step is proved by the EDX analysis, which shows no presence of iodine and 5.4% of fluorine in the PIL.
2d The product was obtained as a white powder. The thermal decomposition of the PIL shows two subsequent steps. The first starts at 319°C, with a weight loss of 23.2%. The second step starts at 418°C and leads to the 21.2% of the starting weight. FT-IR bands assigned to BF_4^- anion appear at 1060 cm^{-1} and 3152 cm^{-1}. The achievement of the ion exchange steps is proved by the EDX analysis which shows no presence of iodine and 13.0% of fluorine in the PIL.

3 Results and discussion

The non-ionic co-polymers were obtained with a precipitation polymerization method[34], using vinylimidazole as functional monomer and divinylbenzene as cross-linking agent as described in the experimental section. Briefly, the two monomers were polymerized using acetonitrile as solvent and toluene as porogen, in order to achieve a permanent porous structure. This method allows to tune the composition of the final co-polymer by varying the ratio between the two monomers thus modulating its physico-chemical properties. The most promising polymers were obtained at the nominal volume ratio of DVB:VIm of 5:5 and 3:7: Poly(DVB-co-VIm)-5:5 (sample **1**) and Poly(DVB-co-VIm)-3:7 (sample **2**), respectively. The synthetic pathway and abbreviations are shown in Scheme 1.

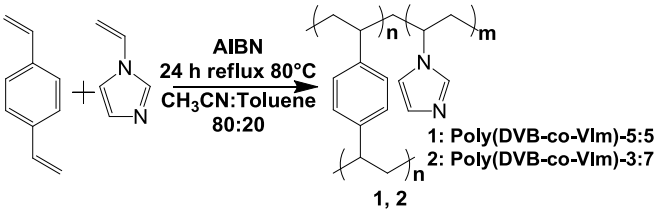

Scheme 1. Polymerization reaction for the non-ionic polymers to give sample **1** and sample **2**

The kinetic of polymerization (*Kp*) of the two monomers is different, but since it depends on a plenty of factors, (e.g. type of monomer, concentration, solvent, temperature) it was difficult to predict the reactivity of the reaction mixture.[35, 36] However, since the DVB has a double functionality, potentially it has a higher *Kp*, leading to a co-polymer with DVB loading higher than the nominal one. Hence, elemental analysis was performed on the non-ionic polymers in order to estimate the real loading of VIm in the resulting polymer. The results are shown in Table 1. For both the co-polymers, the VIm loading in mmol is nearly 10% of the nominal one, suggesting that the different kinetics of polymerization between the two co-monomers leads to an overloading of DVB which is proportional to the nominal concentration. It is worth noting that Poly(DVB-co-VIm)-3:7 contains an amount of VIm which

is one of the largest ever reported in literature for similar co-polymers (in average 1 mmol VIm/g).[24, 37]

Table 1. Elemental analysis of co-polymers **1** and **2** and estimated VIm loading

Entry	% N	% C	% H	mmol Vim/g	% of nominal loading
1	2.47	87.0	7.65	0.88	7.97
2	4.47	83.5	7.42	1.60	10.3

The ionic co-polymers were then obtained from the corresponding non-ionic ones through a quaternarization process (microwave heating in a sealed tubes), as shown in Scheme 2, using alkylating agents differing in the length of the alkyl chain (R) and in the nature of the halogen (X). In particular, methyl iodide, butyl iodide and butyl bromide were used to obtain respectively poly(DVB-co-mVIm$^+$I$^-$) (**1a**, **2a**), poly(DVB-co-bVIm$^+$I$^-$) (**1b**, **2b**), poly(DVB-co-bVIm$^+$Br$^-$) (**1c**, **2c**). In order to prove the completeness of the quaternarization step EDX microanalyses were performed on the obtained PILs. The percentage of iodine in PILs was converted into iodine loading in mmol/g , which is strictly related to the content of ionic liquid moieties. The results, summarized in Table 2, demonstrate that, within the experimental error, a the imidazole units are all converted into ionic liquids units.

Table 2. Iodine content in PILs **1a** and **2a** as determined by EDX microanalysis and estimated VIm loading.

Entry	% I	mmol I/g	% of alkylated VIm
1a	11.1	0.87	99.4
2a	20.1	1.58	99.0

Successively, anion exchange was used to further modify the anionic moieties, that is one of the pivot factor for the IL chemical behavior and stability.[38] In particular, $NaBF_4$ was used to obtain poly(DVB-co-mVIm$^+$BF$_4^-$) (**1d**, **2d**). The completeness of the anion exchanges on the PILs were proven by means of EDX microanalysis. As shown in Table 3, after the anion exchange the percentage of iodine is null in both the PILs, whereas the content of fluorine evidences an almost complete exchange. It is important to consider that the bias for the quantification of fluorine using EDX is higher than iodine, due to its lightweight.

Table 3 Iodine and fluorine contents in PILs **1a** and **2a** as determined by EDX microanalysis and estimated VIm loading

Entry	% I	% F	mmol BF_4^-/g	% of exchanged mVIm$^+$
1d	-	5.4	0.71	81.6
2d	-	13.0	1.71	108.2

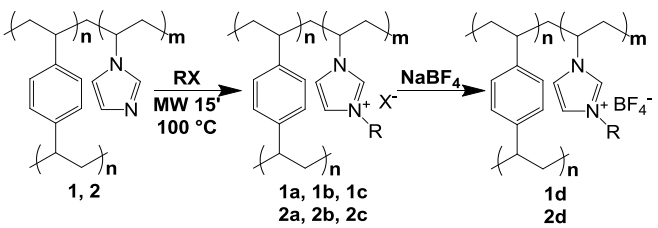

Scheme 2. Synthetic pathway for the PILs used in this work

Table 4. List of the investigated non-ionic polymers and PILs

Entry	RX	Materials
1	-	Poly(DVB-co-VIm) 5:5
1a	MeI	Poly(DVB-co-mVIm$^+$I$^-$) 5:5
1b	BuI	Poly(DVB-co-bVIm$^+$I$^-$) 5:5
1c	BuBr	Poly(DVB-co-bVIm$^+$Br$^-$) 5:5
1d	$MeBF_4$	Poly(DVB-co-mVIm$^+$BF$_4^-$)-5:5
2	-	Poly(DVB-co-VIm) 3:7
2a	MeI	Poly(DVB-co-mVIm$^+$I$^-$) 3:7
2b	BuI	Poly(DVB-co-bVIm$^+$I$^-$) 3:7
2c	BuBr	Poly(DVB-co-bVIm$^+$Br$^-$) 3:7
2d	$MeBF_4$	Poly(DVB-co-mVIm$^+$BF$_4^-$)-3:7

3.1 Non-ionic polymers and PILs vibrational properties

IR spectroscopy in ATR mode was employed as a fast tool to confirm the composition of the co-polymers before and after the quaternarization step. The ATR-FTIR spectra, collected in air, of the two homo-polymers poly(DVB) and poly(VIm), and of co-polymer **1** are compared in Figure 1, whereas the spectrum of co-polymer **2** is reported in Figure 1S, together with the full range FT-IR spectra of the previous polymers.

At high wavenumbers values, the spectrum of poly(VIm) (Figure 1a) shows sharp absorption bands due to CH_x stretching modes of CH_x groups belonging to both the polymer backbone and the VIm ring. These bands are overlapped to a broad absorption band due to (O-H) stretching of the adsorbed H_2O that is significantly present in poly(VIm) because of the high concentration of imidazole, which confers high hydrophilic properties to the poly(VIm). The 1600-600 cm^{-1} region is dominated by the bands related to the bending modes of the imidazole ring and represents the most important part of the spectrum; the major IR fingerprints are evidenced by vertical dot dashed lines in Figure 1 (a)-(c). Particular attention is focused on: (i) the intense band at 1225 cm^{-1}, which is due to the combination of δ(C-C) and δ(C-N) modes of the imidazole ring; (ii) the band at 662 cm^{-1}, assigned to the combination of ν(C-N) and δ ring modes; (iii) the two signals related to the δ(C-H) vibrational modes of the imidazole ring at 1110 cm^{-1} and to δ(C-H) mode combined to the stretching mode of imidazole ring at 1081 cm^{-1}.[39] The spectrum of polyDVB (Figure 1c) shows the absorption bands characteristic of the CH_x stretching modes in the 2800-3100 cm^{-1} region, whereas the absorption bands in the 1600-600 cm^{-1} region are mainly dominated by the bending modes characteristics of a di-substituted benzene. The spectrum of co-polymer **1** (Figure 1b) is very close to that of the poly(DVB), in agreement with the low amount of VIm incorporated during the synthesis (see Table 1). Nevertheless, the presence of VIm in the co-polymer is testified by the observation of the four characteristic absorption bands at 1225, 1110, 1081 and 662 cm^{-1}. These bands are more intense relative to those characteristic of DVB in the spectrum of co-polymer **2** (Figure S1), in agreement with the larger amount of VIm.

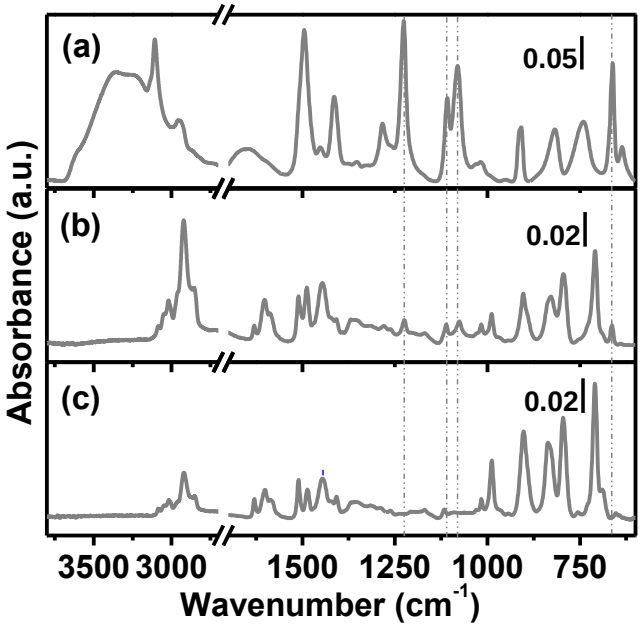

Figure 1. IR-ATR spectra of poly(VIm) (part a); co-polymer **1** (part b) and poly(DVB) (part c). Vertical lines evidence the position of the absorption bands which are the fingerprints of the imidazole ring.

After the quaternization process (Scheme 2), only the VIm vibrational modes are perturbed, whereas the DVB modes appear almost unchanged. This is exemplified in Figure 2 where the ATR-IR spectrum of sample **2** (black curve) is compared to that of the corresponding PIL **2a** (grey curve, alkylated using MeI). The two spectra, in fact, are perfectly overlapped in the vibrational regions characteristic of DVB (which is not involved in the alkylation reaction), whereas the absorption bands characteristic of VIm are significantly perturbed (most relevant changes are underlined by asterisks). In particular, the band assigned to the combined δ $(C\text{-}C)_{ring}$+ δ $(C\text{-}N)_{ring}$ bending modes of the imidazole ring shifts at 1157 cm^{-1} due to the change in the structural configuration of the N3 of the VIm ring. Another spectral evidence of the successful alkylation steps is the shift of the band related to combined ν(C-N) + δ ring modes of the imidazole ring from 662 to 618 cm^{-1}. After the alkylation step the polymer becomes more hydrophilic, as demonstrated by the appearance in the ATR-IR spectrum of a broad absorption band around 3500 cm^{-1}, which is due to the ν(OH) of physisorbed water; that is a consequence of the presence of a formal charge along the chain. In principle, the hydrophilic properties of poly(IL)s are tunable by changing the anion. Indeed, the spectra of **1b**, **1c** and **1d** testify that the water affinity of the co-polymers follows the hydrophilicity of the anions: $Br^- > I^- > BF_4^-$.[40]

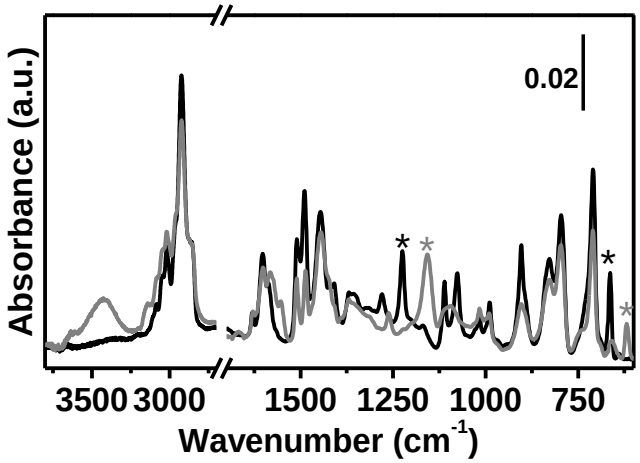

Figure 2. IR-ATR spectra of co-polymer **2** (black) and its corresponding PILs **2a** (grey). The asterisks highlight the shift of the bands characteristic of VIm after the alkylation reaction.

Finally, the ATR-IR spectra shown in Figure S2 allow to confirm the occurrence of anion exchange from **1a** to **1d** and from **2a** to **2d.** The vibrational features of the polymers do not change in most of the wavenumbers region, since the polymeric backbone passes unaltered the exchanging steps. However, a broad band at 1060 cm^{-1}, assigned to the asymmetric vibrational modes of BF_4^-,[41] and a band at 3152 cm^{-1}, due to a combined stretching mode of the cationic imidazole ring and BF_4^- pairs,[42, 43] clearly testify the presence of BF_4^- anion in the exchanged PILs.

3.2 Thermal stability

The thermal stability of sample **1** and **2** and those of their corresponding PILs were evaluated by means of TGA measurements. The main results are summarized in Table 5, whereas the thermogravimetric profiles are shown in Figure 3S. It is evident that neutral polymers are stable in nitrogen up to 400°C. In fact no significant loss in weight is appreciable until this temperature and a similar behavior was found for Poly(DVB). Hence, the introduction of the imidazole functionality along the chain does not affect the stability of the cross-linked system. The PILs with halogens counter-ions, instead, show a weight loss ascribable to the loss of the ionic functionality starting around 170-190 °C depending on the PIL, except for **2b** that is thermally stable until 220°C. After the weight loss ascribed to the decomposition of IL functionality, all the PILs behave as the starting non-ionic polymer. These results are in line with those reported in literature for similar PILs.[23]

Differently to the others PILs, **1d** and **2d** show higher thermal stability, since the decomposition of the ionic liquid moiety starts at about 320°C, indicating that thermal decomposition that generate methylium tetrafluoroborate moiety occurs at higher temperature and in the meanwhile of the polymeric matrix decomposition. The weight losses are directly proportional to the weight of the ionic moiety that decomposes during the thermal ramp up to 500 °C, as summarized in Table 5. As an example, the weight losses for the PILs of series **2** (see Figure S3 for the TGA plot) is larger than the ones of series **1**, in agreement with the higher VIm loading.

Table 5. PILs weight losses as obtained from TGA analysis

Entry	Weight loss %	T onset °C
1a	8.90	172
1b	14.3	189
1c	9.40	187
1d	11.2	323
2a	17.8	178
2b	21.3	219
2c	17.3	207
2d	23.2	319

3.3 Textural and morphological properties

The surface area and the porosity of all the investigated samples, as evaluated by analysis of N_2 volumetric measurements at 77 K, are summarized in Table 6. The two non-ionic polymers show a remarkable high specific surface area (BET), 806 m^2/g for **1** and 709 m^2/g for **2** that, to a large extent, is preserved after the introduction of the IL functionalities. The surface area of all the PILs remain higher than 400 m^2/g, indicating that the PILs synthesized starting from non-ionic polymers retain high porosity.

For what concerns the **1** PILS group, it is observed (accordingly to qualitative expectations) that the longer is the alkyl chain and larger is the anion, the lower is the specific surface area of the corresponding PIL.[29] On the contrary, in the **2** PILs group, an increase in the specific surface area is observed if longer alkali chain or larger anion is present in the material. This fact could be explained by the larger ability to swell for polymers derived by **2** with respect to the ones derived by **1**, because of the lower degree of crosslinking (lower DVB). The presence of larger anions/longer alkyl chains would then induce a larger swelling of the polymers with a corresponding increase in the pore volume due to the creation of mesoporosity. In agreement with this explanation, the isotherms obtained for the **2b** and **2c** polymers are of IIb type, typical of layered materials, whereas those of **1b** and **1c** polymers show IIa type isotherms, being the hysteresis loop almost absent. Moreover, the micropore volume follows the same dependence upon functionalities for both the PILs series, that is the expected decrease with the dimension and weight of the introduced functional groups.

The qualitative analysis of the N_2 isotherms shapes (Figure S4), reveals that all the non-ionic polymers and the corresponding PILs are characterized by the presence of both micropores and mesopores. This was confirmed by the QSDFT analysis (see figure S5) indicating that the micropore region shows a bimodal distribution with two bands centered at 0.7 nm and 1.3 nm, whereas the distribution of the mesopores decreases constantly on increasing the pore size. The coexistence of micropores and mesopores in the polymers is expected to be beneficial for catalytic application of these polymers, since it allows to combine the high specific surface area characteristic of microporous materials with satisfactory mass transfer properties characteristic of mesoporous materials.[44]

The ratio between the micropore volume and the total pore volume is approximately constant (25%) for all the materials, except for **2b** which has a lower ratio (7%). The lower amount of micropores in **2b** may be ascribable on one hand to a larger steric-hindrance due to the co-presence of the longer alkyl chains and of iodine anions (lower micropore volume) and, on the other hand to the larger swelling expected in this polymer with respect to the others (higher mesoporous volume).

Sample morphology was investigated by means of SEM. Representative SEM images of the non-ionic co-polymers **1** and **2** and of the corresponding PILs (**1a** and **2a**) are shown in Figure 3. The microstructure of the polymers is not altered by the alkylation reaction, for both the PILs series. Polymer **1** (Figure 3a) and the corresponding **1a** (Figure 3b) are constituted by round shaped particles, having a narrow distribution centered at about 5 µm.

Table 6. Specific surface area and pore size of all the co-polymers obtained by N_2 adsorption at 77 K

Entry	Surface area m^2/g		Total pore volume[1] cm^3/g	Micropore Volume[2] cm^3/g
	BET	Langmuir		
1	806	1106	0.449	0.115
1a	584	797	0.306	0.096
1b	513	697	0.293	0.071
1c	542	743	0.309	0.079
1d	607	829	0.302	0.094
2	709	973	0.478	0.084
2a	370	506	0.247	0.055
2b	482	668	0.355	0.025
2c	425	585	0.277	0.046
2d	405	549	0.323	0.061

[1] Total pore volume estimated as the liquid N_2 at $p/p_0 \cong 0.97$
[2] Micropore volume obtained from t-plot using the Harkins and Jura thickness equation[32, 33]

The particles are well dispersed and they form only a few aggregates constituted of a low number of particles. The morphology of the non-ionic polymer and PIL obtained with 3:7 ratio is completely different from the ones with 5:5 ratio. Both **2** (Figure 3c) and **2a** (Figure 3d) show particles with a sphere-like morphology but having irregular surfaces. The particles size is of about 300 nm with a narrow distribution. Due to their small particles size, the particles are aggregated in the form of large micro-particles. The differences in

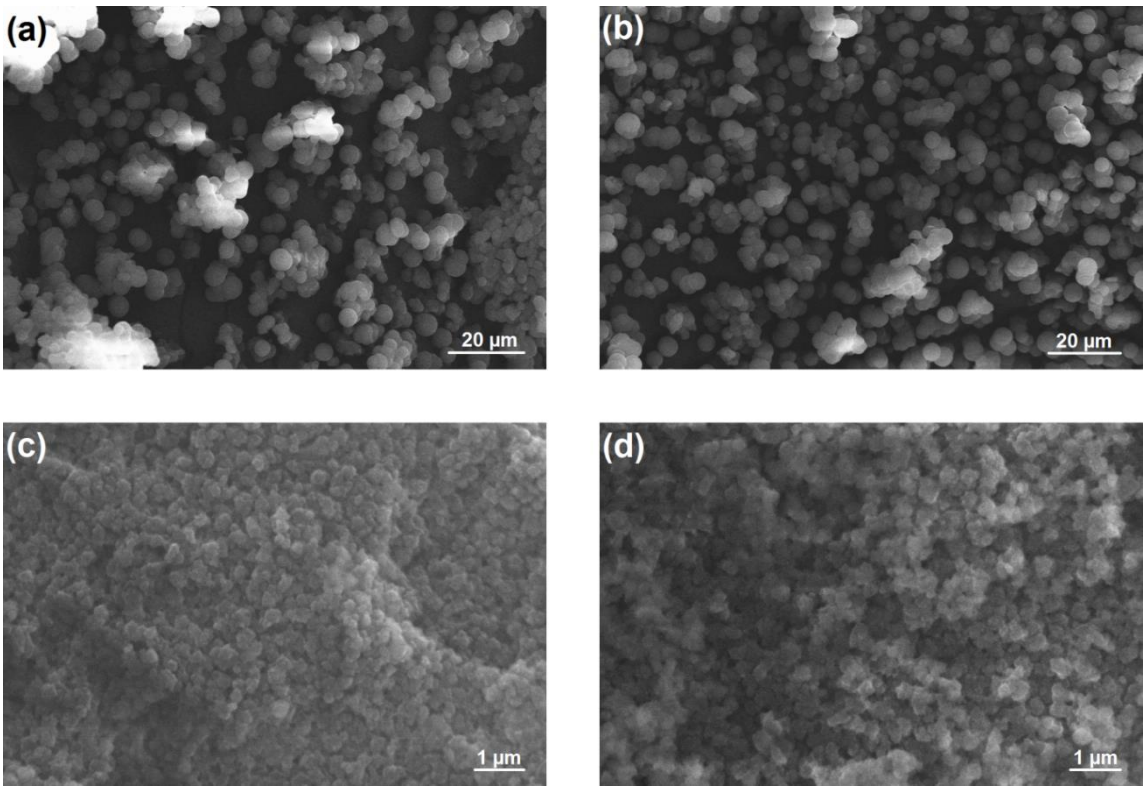

Figure 3. Representative SEM images of samples **1** (part a); **1a** (part b); **2** (part c) and **2a** (part d)

morphology between samples **1** and **2** are ascribable to the different loading of the two co-monomers. The aspect of the former is closer to that of Poly(DVB) (Figure S6a), while the higher loading of imidazole in **2** leads to a polymer having particles with an aspect closer to the poly(VIm) (Figure S6b).

3.4 PILs as efficient catalysts in the coupling reaction between CO_2 and ethylene oxide

The performance of PILs and of the non-ionic polymers in the coupling reaction between CO_2 and ethylene oxide was monitored by *in-situ* FT-IR spectroscopy in transmission within 14 hours of reaction. At the end of the reaction all the samples were outgassed for 30 minutes in order to evaluate the fraction of reversibly adsorbed species (see experimental for the detailed procedure). Figure 4 shows the FT-IR spectrum of polymer **2b**, chosen here as an example. Spectra were collected before the reaction (spectrum a), in presence of a mixture of CO_2 and ethylene oxide (spectrum b), after 14 hours of reaction (spectrum c) and after removal of the un-reacted reagents and removable products (spectrum d). The spectrum of the starting polymer (spectrum a) is the same as collected in ATR, except for the presence of a scattering profile and for the absence of the broad absorption band around 3500 cm^{-1} because of the removal of adsorbed H_2O. In presence of the reaction mixture (spectrum b), absorption bands related to the reagents appear in the spectrum: in particular at 3065 and 859 cm^{-1} due to gaseous ethylene oxide and at 2350 cm^{-1} (ν_{as} (O=C=O) due to gaseous CO_2).

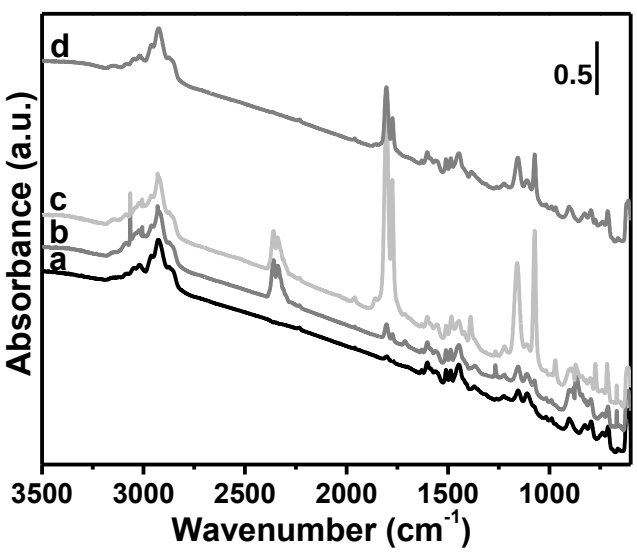

Figure 4. FTIR spectra of sample **2b** before reaction (spectrum a), immediately after contact with the mixture of ethylene oxide and carbon dioxide (spectrum b), after 5 hours in presence of the reaction mixture (spectrum c), and after prolonged degassing at room temperature (spectrum d). The spectra are reported vertically translated for the sake of simplicity.

After some hours since the start of the experiment (spectrum c) a consistent amount of ethylene carbonate (EC) is obtained, as testified by the presence of a doublet of bands at 1805 cm^{-1} and 1774 cm^{-1} that can be easily ascribed to the combined carbonyl stretching modes of the ethylene carbonate. Most of the formed

EC is easily removed by a simple degassing at room temperature, with the consequent regeneration of the catalytic active sites (spectrum d in Figure 4).

The whole sequence of spectra recorded during the reaction, at a time resolution of 50 minutes are shown in Figure 5 after subtracting spectrum a). Also the FT-IR spectrum of ethylene carbonate is shown for comparison; it is evident that all the absorption bands growing in the spectra during the reaction are due to ethylene carbonate and there are no side products. The integrated area of the band at 1805 cm^{-1}, proportional to the EC yield, was monitored as a function of time in order to obtain a kinetic profile of the reaction. As shown in Figure 6 it is evident that the coupling reaction starts immediately after the two reagents are put in contact with the PIL catalysts. This is quite interesting since, differently from previous studies, the reaction is performed in mild conditions (room temperature and low pressure, about 200 mbar).

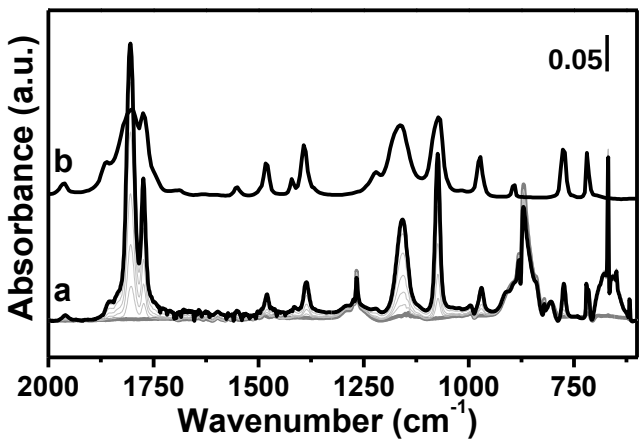

Figure 5. Part a): Sequence of FT-IR spectra collected during reaction of EC and CO_2 on sample **2b**, collected at a time resolution of 50 minutes, after subtraction of spectrum 1 of Figure 5. Part b): spectrum of pure EC.

Similar results were obtained for all the PILs. It was found that the yield of EC (evaluated from the intensity of the characteristic band at 1805 cm^{-1}) depends on the loading of VIm. Thus, for an equal mass of PILs, the best catalytic performances are observed for the PILs of series **2**, because of the higher content of VIm per gram of PILs. By normalizing the FT-IR spectra to the imidazole content it is possible to look at the catalytic properties relatively to the number of the active sites. Hence, the FT-IR spectra were normalized as follows: a) within the same series (**1** or **2**), the spectra were normalized to the amount of DVB (i.e. imposing the same height for the doublet of bands at 1486 cm^{-1} and 1510 cm^{-1}), to account for the different thickness of the sample; b) to compare the data for samples of the two series, the spectra were further normalized for the effective amount of Vim (determined from the intensity of the bands at 1158 cm^{-1} (ascribable to the combination of δ(C-C) and δ(C-N) modes of the imidazole ring). The results reported in Figure 6 show that, by normalizing to the amount of imidazole, the EC yield is of the same order of magnitude for PILs of series **1** and **2**. This means, in turn, that the active site is the same, and the porosity of the samples is enough to guarantee a sufficient accessibility of the active sites for both the two series.

Going in more details, among PILs of series **1**, the one containing iodine as anion has the higher activity. The catalyst activity follows the nucleophilicity of the anion (I^->Br^-). These results are easily explainable by considering that the first step

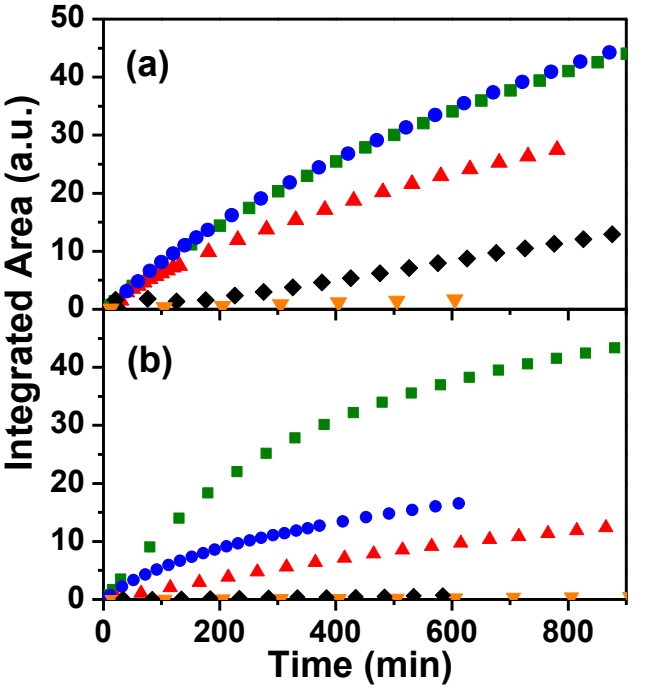

Figure 6. Integrated area of the IR absorption band at 1805 cm^{-1} (corresponding to the EC yield) monitored as a function of reaction time for all the samples analyzed in this work. Parts a) and b) refer to PILs of series **1** and **2**, respectively. **1** and **2** black diamond, **1a** and **2a** blue sphere, **1b** and **2b** green square, **1c** and **2c** red top up triangle, **1d** and **2d** orange top down triangle.

of the reaction is the ring-opening of ethylene oxide, which is favored in presence of more nucleophilic anions.[23, 25] In series **1,** almost no differences in the reaction rate are found by changing the alkyl chains. On the contrary, for PILs of series **2**, the length of the alkyl chain affects the reaction rate. Longer alkyl chains stabilize the imidazole cation and reduce the electrostatic attraction between the ion-pair, so that the anion is more available to catalyze the reaction, as reported in literature for ILs.[19] Finally, both PILs with BF_4^- show no reactivity at all towards the coupling reaction. This lack of catalytic activity is not ascribable to some confinement effect due to the bulkiness of the cation, since the pore size and the total pore volume of **1d** and **2d** is pretty the same of the starting materials **1a** and **2a.** Hence this leak of reactivity is mainly due to the low nucleophilicity of BF_4^- anion, due to the high delocalized charge, which is not sufficient to allow the ring opening of ethylene oxide.[28] This is another important evidence of the need for a nucleophilic agent in the first step of the reaction.

The same experiment was repeated for Poly(DVB), non-ionic co-polymers, and Poly($mVIm^+I^-$) for comparison. For Poly(DVB) no production of EC was found, demonstrating that the catalysis is not induced by a constraint effect of the two reagents operated by high surface area and porosity of the polymeric matrix. On the non-ionic co-polymers, no reactivity is observed within the first two hours. For longer times, the reaction gradually starts, but the EC yield is very low compared to PILs.[25, 26] Hence, also the imidazole moiety may catalyze the coupling reaction, probably through the electron doublet at the N3 that act as a nucleophile, and thus facilitates the opening of

the ethylene oxide ring. The better performances of PILs must be attributed to the concomitance of two factors: a greater localization of the negative charge in the anion, which promotes the opening of the EO ring, and the presence of a localized positive charge on the imidazole, acting as activator for carbon dioxide. Finally, on the Poly(mVIm$^+$I$^-$) the observed reactivity was very low, despite the higher concentration of active sites, as a consequence of the absence of porosity and then of the low accessibility to the active sites (see Figure S7). PILs showed to be stable along the reaction and did not reveal any loss in iodine content (EDX measurements).

4 Concluding remarks

A set of imidazole-based PILs characterized by different alkyl chains, different anions and crosslink degree were successfully synthesized and fully characterized. This original synthetic approach opens an easy route to obtain different PILs starting from the same non-ionic copolymer, allowing to systematically investigate the effect of each single component on the properties of the materials.

The synthetized PILs displayed excellent catalytic performances in the coupling of carbon dioxide and ethylene oxide to give ethylene carbonate in mild conditions (low pressure and room temperature). The easiness of the synthetic pathway and the low cost of the raw materials are good premises for a future application of these PILs in the industrial catalytic production of ethylene carbonate.

The reaction was followed in situ by means of FT-IR spectroscopy, which has proven to be a valuable method to compare reaction rates and to evaluate reaction yields. It was found that the catalytic performances of a PIL depend on the presence of a sufficient surface area and are proportional to the VIm content, that can be considered as the active catalytic site. Localization of the electronic charges is the key factor to promote reactivity. Hence, catalyst's activity increases with increasing the nucleophilicity of the anion and for longer alkyl chains (which stabilize the imidazole cation).

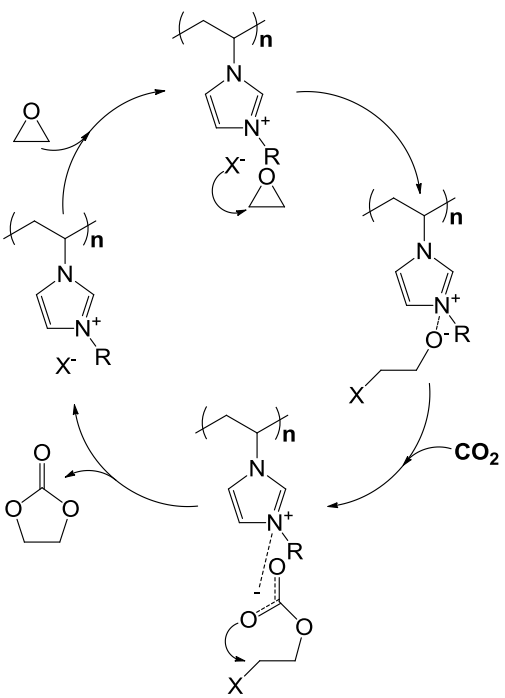

Scheme 3. Proposed scheme of the catalytic steps which occur in the reaction between carbon dioxide and ethylene oxide to produce ethylene carbonate over a PIL catalyst.

However, the activity declines when steric factors become important (too large anions, too long alkyl chains), because the accessibility of the reagents to the active sites is limited.

The proposed reaction steps are reported in Scheme 3. The first step is the ring opening of ethylene oxide driven by the anion (step 1). The incipient negative charge on the oxygen atom is then stabilized by the imidazole cation (step 2). Then carbon dioxide is activated by the negative charge of oxygen and a new C-O bond is formed; the negative charge is transferred to the two oxygen atoms of carbon dioxide and is stabilized by resonance and by the interaction with the imidazole cation (step 3). Subsequently the oxygen bringing the negative charge attacks the carbon bearing the anion, closing the cycle and restoring the catalytic site (step 4). The non-ionic polymers may exploit a similar catalytic cycle where the electronic doublet of imidazole is the nucleophile promoting the reaction.

Acknowledgement

MIUR-PRIN 2010-2011 (project n:2010A2FSS9) is kindly acknowledged for the financial support.
Federica Franconieri is acknowledged for the SEM imagines.

Notes and references

[a] *Department of Chemistry, NIS and INSTM Reference Centres, University of Torino, Via Quarello 15 A, Torino 10135, Italy.*
E Mail:silvia.bordiga@unito.it
[b] *Department of Science and High Technology, Università dell'Insubria, Via Lucini 3, 22100 Como, Italy*

Electronic Supplementary Information (ESI) available: IR-ATR spectra of homo-polymers and co-polymers, IR-ATR spectra of PILs, Thermo Gravimetric Analysis, Adsorption and Desorption isotherms in N_2 at 77K, pore size distribution obtained from QSDFT, SEM images of homo-polymer. See DOI: 10.1039/b000000x/

1. K. M. K. Yu, I. Curcic, J. Gabriel and S. C. E. Tsang, *ChemSusChem*, 2008, **1**, 893-899.
2. R. Zevenhoven, S. Eloneva and S. Teir, *Catalysis Today*, 2006, **115**, 73-79.
3. A. Dibenedetto, A. Angelini and P. Stufano, *Journal of Chemical Technology & Biotechnology*, 2014, **89**, 334-353.
4. http://www.esrl.noaa.gov/gmd/ccgg/trends/, 2014.
5. M. Mikkelsen, M. Jorgensen and F. C. Krebs, *Energy & Environmental Science*, 2010, **3**, 43-81.
6. D. M. D'Alessandro, B. Smit and J. R. Long, *Angewandte Chemie International Edition*, 2010, **49**, 6058-6082.
7. E. A. Quadrelli, G. Centi, J.-L. Duplan and S. Perathoner, *ChemSusChem*, 2011, **4**, 1194-1215.
8. K. Sumida, D. L. Rogow, J. A. Mason, T. M. McDonald, E. D. Bloch, Z. R. Herm, T.-H. Bae and J. R. Long, *Chemical Reviews*, 2012, **112**, 724-781.
9. T. Sakakura, J.-C. Choi and H. Yasuda, *Chemical Reviews*, 2007, **107**, 2365-2387.

10. D. J. Darensbourg and M. W. Holtcamp, *Coordination Chemistry Reviews*, 1996, **153**, 155-174.
11. S. Jagtap, M. Bhanushali, A. Panda and B. Bhanage, *Catalysis Letters*, 2006, **112**, 51-55.
12. N. Kihara, N. Hara and T. Endo, *The Journal of Organic Chemistry*, 1993, **58**, 6198-6202.
13. S.-S. Wu, X.-W. Zhang, W.-L. Dai, S.-F. Yin, W.-S. Li, Y.-Q. Ren and C.-T. Au, *Applied Catalysis A: General*, 2008, **341**, 106-111.
14. H. Yasuda, L.-N. He and T. Sakakura, *Journal of Catalysis*, 2002, **209**, 547-550.
15. A. Dibenedetto, M. Aresta, F. Nocito, C. Pastore, A. M. Venezia, E. Chirykalova, V. I. Kononenko, V. G. Shevchenko and I. A. Chupova, *Catalysis Today*, 2006, **115**, 117-123.
16. J. Roeser, K. Kailasam and A. Thomas, *ChemSusChem*, 2012, **5**, 1793-1799.
17. R. L. Paddock and S. T. Nguyen, *Journal of the American Chemical Society*, 2001, **123**, 11498-11499.
18. H. S. Kim, J. J. Kim, B. G. Lee, O. S. Jung, H. G. Jang and S. O. Kang, *Angewandte Chemie International Edition*, 2000, **39**, 4096-4098.
19. H. Kawanami, A. Sasaki, K. Matsui and Y. Ikushima, *Chemical Communications*, 2003, 896-897.
20. J. Sun, S.-i. Fujita and M. Arai, *Journal of Organometallic Chemistry*, 2005, **690**, 3490-3497.
21. S. Zhang, Y. Chen, F. Li, X. Lu, W. Dai and R. Mori, *Catalysis Today*, 2006, **115**, 61-69.
22. T.-Y. Shi, J.-Q. Wang, J. Sun, M.-H. Wang, W.-G. Cheng and S.-J. Zhang, *RSC Advances*, 2013, **3**, 3726-3732.
23. L. Han, H.-J. Choi, D.-K. Kim, S.-W. Park, B. Liu and D.-W. Park, *Journal of Molecular Catalysis A: Chemical*, 2011, **338**, 58-64.
24. Y. Xie, Z. Zhang, T. Jiang, J. He, B. Han, T. Wu and K. Ding, *Angewandte Chemie International Edition*, 2007, **46**, 7255-7258.
25. J. Sun, W. Cheng, W. Fan, Y. Wang, Z. Meng and S. Zhang, *Catalysis Today*, 2009, **148**, 361-367.
26. W.-L. Dai, L. Chen, S.-F. Yin, W.-H. Li, Y.-Y. Zhang, S.-L. Luo and C.-T. Au, *Catalysis Letters*, 2010, **137**, 74-80.
27. Y. Zhang, S. Yin, S. Luo and C. T. Au, *Industrial & Engineering Chemistry Research*, 2012, **51**, 3951-3957.
28. S. Ghazali-Esfahani, H. Song, E. Paunescu, F. D. Bobbink, H. Liu, Z. Fei, G. Laurenczy, M. Bagherzadeh, N. Yan and P. J. Dyson, *Green Chemistry*, 2013, **15**, 1584-1589.
29. F. Liu, L. Wang, Q. Sun, L. Zhu, X. Meng and F.-S. Xiao, *Journal of the American Chemical Society*, 2012, **134**, 16948-16950.
30. A. Wilke, J. Yuan, M. Antonietti and J. Weber, *ACS Macro Letters*, 2012, **1**, 1028-1031.
31. K. T. Prabhu Charan, N. Pothanagandhi, K. Vijayakrishna, A. Sivaramakrishna, D. Mecerreyes and B. Sreedhar, *European Polymer Journal*, 2014, **60**, 114-122.
32. S. J. Gregg and K. S. W. Sing, *Adsorption, surface area, and porosity*, Academic Press, London; New York, 1982.
33. W. D. Harkins and G. Jura, *Journal of the American Chemical Society*, 1944, **66**, 1362-1366.
34. M. T. Gokmen and F. E. Du Prez, *Progress in Polymer Science*, 2012, **37**, 365-405.
35. S. Beuermann, M. Buback, P. Hesse, S. Kukučková and I. Lacık, *Macromolecular Symposia*, 2007, **248**, 23-32.
36. S. Beuermann and M. Buback, *Progress in Polymer Science*, 2002, **27**, 191-254.
37. N. Fontanals, R. Maria Marcé, M. Galià and F. Borrull, *Journal of Polymer Science Part A: Polymer Chemistry*, 2004, **42**, 2019-2025.
38. G. W. Meindersma, M. Maase and A. B. De Haan, in *Ullmann's Encyclopedia of Industrial Chemistry*, Wiley-VCH Verlag GmbH & Co. KGaA, Editon edn., 2012.
39. J. L. Lippert, J. A. Robertson, J. R. Havens and J. S. Tan, *Macromolecules*, 1985, **18**, 63-67.
40. J. Yuan and M. Antonietti, *Polymer*, 2011, **52**, 1469-1482.
41. L. Yu, J. Clifford, T. T. Pham, E. Almaraz, F. Perry, G. A. Caputo and T. D. Vaden, *The Journal of Physical Chemistry B*, 2013, **117**, 7057-7064.
42. R. Holomb, A. Martinelli, I. Albinsson, J. C. Lassègues, P. Johansson and P. Jacobsson, *Journal of Raman Spectroscopy*, 2008, **39**, 793-805.
43. H. Zine, M. H. Baron and A. Piart-Goypiron, *Spectrochimica Acta Part A: Molecular and Biomolecular Spectroscopy*, 1995, **51**, 457-470.
44. D. Kuzmicz, P. Coupillaud, Y. Men, J. Vignolle, G. Vendraminetto, M. Ambrogi, D. Taton and J. Yuan, *Polymer*, 2014, **55**, 3423-3430.